European Review for Medical and Pharmacological Sciences 2019; 23: 7338-7349

Nanoscale bubble delivered YCD-TK/Cx26 gene therapeutic system suppresses tumor growth by inducing necrosis of tumor tissues in mouse Xenograft bladder cancer models

Y.-R. FU[1], Y. LUO[2], X. XIE[1], W. LU[1], R. ZHANG[1], B. XIONG[3], F. CHEN[1]

[1]Department of Urology, The Peoples Hospital of Nanchuan Chongqing, Chongqing, China
[2]Department of Gynecology and Obstetrics, The First Affiliated Hospital, Chongqing Medical University, Chongqing, China

Abstract. – OBJECTIVE: Bladder cancer is considered as the fifth most common cancer in the whole world. This study aimed to investigate the anti-tumor effects of Nanoscale bubbles delivered yeast cytosine deaminase thymidine kinase/connexin 26 (YCD-TK/Cx26) on tumor cell proliferation and tumor growth.

MATERIALS AND METHODS: Nanoscale bubble was prepared using thin-film hydration-sonication method. Nanoscale bubble-LV5-YCD-TK+PCD-Cx26 was generated and transfected into BIU-87 cells. MTT assay was employed to detect cell viability. Apoptosis was determined using a flow cytometry assay. YCD-TK and Cx26 expressions were detected using Western blot and Real Time-PCR (RT-PCR). BIU-87 cells were transplanted into mice to establish Xenograft models. The tumor volume was recorded. HE staining was used to examine necrosis areas in tumor tissues.

RESULTS: Nanoscale bubble (Nanoscale bubble-LV5-YCD-TK+PCD-Cx26) successfully mediated YCD-TK and Cx26 gene expression in BIU-87 cells. Nanoscale bubble delivered YCD-TK/Cx26 expression significantly inhibited cell viability and induced apoptosis compared to Nanoscale bubble-LV5-YCD-TK and Nanoscale bubble group ($p<0.05$). Nanoscale bubble delivered YCD-TK/Cx26 expression triggered significantly higher levels of bystander effect compared to single YCD-TK or single Cx26 gene ($p<0.05$). Nanoscale bubble delivered YCD-TK/Cx26 expression significantly reduced tumor volume in mouse Xenograft bladder cancer model compared to LV5-YCD-TK and 5-FC+GCV group ($p<0.05$). Nanoscale bubble delivered YCD-TK/Cx26 expression significantly reduced the necrosis of tumor tissues in mouse Xenograft bladder cancer model compared to LV5-YCD-TK group and 5-FC+GCV group ($p<0.05$).

CONCLUSIONS: Nanoscale bubble delivered YCD-TK/Cx26 gene therapeutic system efficiently reduced BIU-87 cell proliferation *in vitro*, and suppressed tumor growth by inducing necrosis of tumor tissues in mouse Xenograft bladder cancer models.

Key Words:
Bladder cancer, Nanoscale bubble, Gene therapy, Xenograft model.

Introduction

Bladder cancer is considered to be the fifth most common cancer, and the second most frequently occurred human genitourinary cancer[1,2]. Meanwhile, both mortality and morbidity for bladder cancer are considered to be the second highest in all urinary tumors, closely following prostate cancer[3]. Bladder cancer is characterized by a higher metastasis rate and is easily recurrent, following by a 5-year survival rate less than 60%[4]. Although many anti-tumor strategies, including surgical resection, chemotherapy or radiotherapy, plenty of unfavorable side effects or resistances, have been extensively discovered[5,6]. In recent years, the multimodal treatments for tumors have been developed with an increasing tendency[7,8], especially for the non-surgical treatment, such as gene therapy, which is the promising approach for cancers[9]. Cancer gene therapy is also a significant and potential therapeutic approach for cancer treatment. Therefore, we believed that the enhancement of the therapeutic efficacy of gene therapy using novel drug-delivery strategies is critical for cancer treatments.

Corresponding Author: Feng Chen, MD; e-mail: yuxunzhoo@sina.com

In the past years, many drug-delivery strategies, such as vectors (viral vector, bacterial vector), bio-adhesive microspheres, anti-sense oligodeoxynucleotides, and magnetically targeted carries[9-12], have been applied to gene carrying vectors for cancer treatment. However, there are also a few obstacles and limitations for above gene delivery strategies, such as toxicity of gene carrier, lower selectivity for tumor cells, and other side-effects.

Nowadays, contrast-enhanced ultrasonography technology has been extensively applied to the tumor treatment according to its capability of targeting normal lesions[13,14]. Especially, recent developed Nanoscale bubble, which is a novel contrast agent for imaging extra-vascular images[15]. The Nanoscale ultrasound contrast agents carrying many cores (such as gas, solid, or liquid) and shells (such as phospholipids or the polymers) have been demonstrated good contrast-enhancement[15]. Previous studies[15,16] reported that Nanoscale ultrasound contrast agents could be applied for contrast-enhanced tumor imaging and demonstrate the promising capability for gene or drug delivery.

The key point for establishing the optimal gene therapy is to develop the tumor-specific targeting therapeutic gene delivery system. Previous studies[17-19] have been reported some efficient gene targeting systems, such as *Bifidobacterium infantis*, tumor-suicide gene therapy system [herpes simplex virus thymidine kinase (HSV-TK) and yeast cytosine deaminase (YCD) system] and thymidine kinase gene targeting system. Till now, the most applied suicide gene therapy system is HSV-TK integrating Ganciclovir (GCV) or YCD integrating 5-fluorocytosine (5-FC)[17,20]. Here, we firstly involved a kind of tumor-suppressor gene, connexin 26 (Cx26)[21], in the tumor-suicide gene therapy system to enhance anti-tumor effects. In the present study, we firstly synthesized the Nanoscale ultrasound contrast agents and then observed the anti-tumor effects of Nanoscale bubbles delivered YCD-TK/GCV/Cx26 or YCD-TK/5-FC/Cx26 on tumor growth of BIU-87-induced mouse Xenograft bladder cancer models.

Materials and Methods

Bladder Cancer Cell Culture and Nanoscale Bubbles Preparation

Human bladder cancer cell, BIU-87, was obtained from Cell Bank of CAS (Shanghai, China) and cultured in Roswell Park Memorial Institute-1640 (RPMI-1640) containing 100 U/ml penicillin and 100 μg/ml streptomycin (Beyotime Biotechnology, Shanghai, China) and supplementing with 10% fetal bovine serum (FBS; Gibco BRL Co. Ltd., Grand Island, NY, USA) in humidified environment with 5% CO_2 at 37°C.

The targeted Nanoscale bubble was prepared using thin-film hydration-sonication method due to the former study described[22], with a few modifications, as our team previously reported[23]. Finally, the synthesized biotinylated-lipid Nanoscale bubbles were incubated using streptavidin (Sigma-Aldrich, St. Louis, MO, USA) at 4°C for 30 min, based on the description of the former description[24]. Nanoscale bubbles were successfully prepared (Figure 1A) and stored for the following experiments.

Plasmids Containing YCD-TK or Cx26 Gene Construction, Lentivirus Packaging

The construction of LV5-YCD-TK plasmid and lentivirus packaging were conducted according to our former study[23]. The Cx26 gene was amplified with the primers (sense-primer: 5'-TCTTCATTTTTCGCATTATG-3', anti-sense-primer: 5'-CATGTCTCCGGTAGGCCACG-3'), generating the 678 bp length Cx26 gene products. The PCR products were cloned into EcoR I-EcoR V sites of pcDNA6/myc-HisA vector (Cat. No. V22120, Invitrogen/Life Technologies, Carlsbad, CA, USA) according to the instruction of the manufacturer. The obtained clone product was named as PCD-Cx26. Then, PCD-Cx26 was amplified in *E. coli* (Tiangen Biotechnology Co. Ltd., Beijing, China), isolated with E.Z.N.A. Fastfiler Endo-free Plasmid Maxiprep Kit (Cat. No. D6948, Omega Bio-Tek, Doraville, GA, USA) and identified using DNA sequencing.

Transfection of Gene Expressing Plasmids Into Nanoscale Bubbles

The plasmid transfection was conducted according to the previous study[23]. Briefly, the Nanoscale bubbles were added to BIU-87 cells at a final concentration of 0.1 μg/μl. The YCD/TK gene (LV5-YCD-TK) and Cx26 gene (PCD-Cx26) were transfected into BIU-87 with Nanoscale bubbles and sonicated for 60 s. Eventually, G418 (Cat. No. PP2374, Sigma-Aldrich, St. Louis, MO, USA), at a concentration of 400 μg/μl, was employed to screen the plasmids positively transfected BIU-87 cells.

3-(4,5-Dimethyl-2-Thiazolyl)-2,5-Diphenyl- 2- H-Tetrazolium Bromide (MTT) Assay

BIU-87 cells were treated with drugs, gene-carrying plasmids, according to the experimental design. The cell viability or cell inhibitive rates were assessed or calculated using MTT assay based on the former report[25]. In brief, BIU-87 cells were treated using the MTT solution (Sigma-Aldrich, St. Louis, MO, USA) at a final dosage of 5 mg/ml for 4 h at 37°C. In order to dissolve the formed crystal, a total of 150 µl dimethyl sulfoxide (DMSO, Amresco Inc., Solon, OH, USA) was administrated to BIU-87 cells for 10 min. Eventually, the optical density value of the products was evaluated using a microplate reader (Thermo Fisher Scientific, Waltham, MA, USA) at 490 nm. Cell viabilities were calculated and analyzed due to the OD recordings in various groups.

Flow Cytometry Assay

In this study, the apoptosis for BIU-87 cells was assessed using flow cytometry assay. The apoptosis was examined with Annexin V-PE/7-AAD apoptosis kit (BD Biosciences, San Jose, CA, USA) due to the manufacturer's instruction. In brief, BIU-87 cells were incubated with Annexin V binding buffer, and then treated using Annexin V-PE and propidium iodide (PI) for 15 min in the dark. The apoptosis cells were observed using FACS Vantage SE flow cytometer (BD Biosciences, Franklin Lakes, NJ, USA). Eventually, the stained cells were captured using a 530/578 filter (monitoring the Annexin V binding cells) and a 546/647 filter (for monitoring PI binding cells).

Quantitative Real Time-PCR (qRT-PCR)

The total RNAs of BIU-87 cells were treated using TRIzol kits (Beyotime Biotechnology, Shanghai, China) according to the instruction of the manufacturer. RNAs products were synthesized to the complementary DNA (cDNA) by employing RNA Transcription Kit (Western Biotechnology, Chongqing, China). The qRT-PCR assay was conducted to evaluate Cx26 gene levels, using SYBR Green I Real-Time PCR amplification system (Western Biotechnology, Chongqing, China), taking the cDNAs as templates. The primers for qRT-PCR assay were listed in Table I. The whole qRT-PCR assay was performed using FTC-3000P Real-Time Fluorescence PCR equipment (Funglyn BioTech Inc., Toronto, Canada). The qRT-PCR was conducted at 94°C, 4 min firstly, and then processed with 35 cycles of 94°C for 20 s, 60°C for 30 s, 72°C for 30 s, and finally terminated for 10 min at 72°C. The $2^{-\Delta Ct\ (2-[(Ct\ of\ gene)-(Ct\ of\ U6)])}$ method[26] was employed to calculate the relative Cx26 gene expression in RT-PCR products.

Western Blot Assay

The BIU-87 cells were lysed with the radioimmunoprecipitation assay (RIPA) buffer, and the obtained lysates were centrifuged for 10 min at 10000×g to harvest the supernatant containing proteins. The supernatants were then separated with 10% sodium dodecyl sulphate-polyAcrylamide gel electrophoresis (SDS-PAGE, Amresco Inc., Solon, OH, USA) and transferred onto polyvinylidene difluoride (PVDF) membranes (Bio-Rad Laboratories, Hercules, CA, USA) using Trans-Blot SD cell instrument (Bio-Rad Laboratories, Hercules, CA, USA). Then, PVDF membranes were incubated using rabbit anti-human TK polyclonal antibody (1: 2000; Cat. No. ab129880, Abcam Biotechnology, Cambridge, MA, USA), mouse anti-human Cx26 monoclonal antibody (1:3000, Cat. No. sc-293223, Santa Cruz Biotechnology, Santa Cruz, CA, USA) and rabbit anti-human β-actin antibody (1: 3000; Cat. No. ab8226, Abcam Biotechnology, Cambridge, MA, USA) at 4°C overnight. Then, PVDF membranes were continuously incubated with Horse Radish Peroxidase (HRP)-conjugated goat anti-mouse IgG (1: 2000, Sigma-Aldrich, St. Louis, MO, USA) and HRP-labeled goat anti-rabbit IgG (1: 2000, Sigma-Aldrich, St. Louis, MO, USA) at 37°C for 60 min. Finally, the Western blotting bands were determined using an enhanced che-

Table I. The primers for the RT-PCR assay.

Gene		Sequences	Length (bp)
Cx26	Forward	5'-TTCGCATTATGATCCTCGTTG-3'	122
	Reverse	5'-GATGGGGAAGTAGTGATCGTAGC-3'	
β-actin	Forward	5'-TGACGTGGACATCCGCAAAG-3'	205
	Reverse	5'-CTGGAAGGTGGACAGCGAGG-3'	

miluminescence (ECL) kit (Thermo Scientific Pierce, Rockford, IL, USA) in the dark for 2 min. The relative grey density for the Western blotting bands was calculated with Labworks™ Analysis Software (Labworks, Upland, CA, USA).

Mouse Xenograft Model Establishment

In this study, mouse Xenograft bladder cancer model was generated using BIU-87 cells (the cells might be preliminarily treated with various plasmids). The BALB/C mice, aging from 4 weeks to 8 weeks and weighting from 15 g to 20 g, were purchased from Beijing Huafukang Bio-Tech Co. Ltd. (Beijing, China). Briefly, the above mice were randomly divided into 5 groups, including the Blank group (n=3, without any treatment), 5-FC+GCV group (n=3, administrated with 5-FC and GCV), LV5-YCD-TK group (administrated with LV5-YCD-TK plasmid), LV5-YCD-TK+5FC+GCV group (n=3, administrated with both of LV5-YCD-TK plasmid and 5FC/GCV), and LV5-YCD-TK+PCD-Cx26+5-FC+GCV group (n=3, administrated with LV5-YCD-TK plasmid, PCD-Cx26 plasmid and 5FC/GCV). All mice were housed in specific pathogen free (SPF) conditions. For all mice in the above groups, the above treated BIU-87 cells (at a density of 1×10^7 cells) were injected into the right flank of mice. All growth of mice was monitored, and the tumor width and tumor length were recorded every week. After all *in vivo* experiments, all mice were euthanized, and the tumor tissues were removed for the following histological analysis.

All protocols for the animal experiments have been approved by the Ethics Committee of the People's Hospital of Nanchuan Chongqing (Chongqing, China).

Hematoxylin and Eosin (HE) Staining

The tumor tissues were extracted and fixed with 4% paraformaldehyde (Sangon Biotechnology, Shanghai, China) for 20 min at room temperature. Then, the tumor tissues were sliced into sections with a thickness of 5 μm, and the endogenous peroxidase was inactivated using 3% hydrogen peroxide for 10 min. The histology of tumor tissue sections was visualized using eosin (Beyotime Biotechnology, Shanghai, China) and hematoxylin (Jiancheng Bioengineering Institute, Nanjing, China) as the former study described[27]. The hematoxylin and eosin (HE) stained tumor tissues were imaged using a digital microscope (Mode: DSX110, Olympus, Japan), with a magnification of 200 ×.

Statistical Analysis

The data here were represented as mean ± standard deviation (SD) and analyzed using professional SPSS software (version: 20.0, IBM Corp., Armonk, NY, USA). ANOVA test was used to compare the differences among multiple groups and was validated by Tukey's post-hoc test. The Student's *t*-test was employed to compare the differences between the two groups. All tests or experiments were performed at least 6 times. The $p<0.05$ was assigned as a significant difference.

Results

Nanoscale Bubble Successfully Mediated YCD-TK Gene Expression in BIU-87 Cells

To identify the expression of Nanoscale bubble carried the therapeutic gene, YCD-TK, in BIU-87 cells, Western blotting assay (Figure 1B) was employed for detecting. The finding illustrated that YCD-TK level in the Nanoscale bubble-LV5-YCD-TK group was significantly higher compared to the YCD-TK level in the Nanoscale bubble-LV5 group (Figure 1B, $p<0.05$). This result suggests that LV5-YCD-TK treatment could trigger the overexpression of YCD-TK in BIU-87 cells.

Nanoscale Bubble Mediated Cx26 Gene Expression in BIU-87 Cells

In order to confirm the expression of Nanoscale bubble delivered PCD-Cx26 in the BIU-87 cells, both the qRT-PCR assay and Western blotting assay were conducted. Both the qRT-PCR (Figure 2A) and Western blotting (Figure 2B) results showed that the mRNA and protein expressions in Nanoscale bubble-LV5-YCD-TK+PCD-Cx26 group were higher significantly compared to that in the Nanoscale bubble group and Nanoscale bubble-LV5-YCD-TK group ($p<0.05$). Although BIU-87 cells in both Nanoscale bubble group and Nanoscale bubble-LV5-YCD-TK group expressed Cx26, whose levels in Nanoscale bubble-LV5-YCD-TK group were relatively higher compared to that in the Nanoscale bubble ($p<0.05$).

Nanoscale Bubble Delivered YCD-TK/Cx26 Expression Inhibited Cell Viability and Caused Apoptosis

In this study, we transfected the Nanoscale bubble suicide gene therapy system delivered YCD-TK and Cx-26 gene into BIU-87 cells;

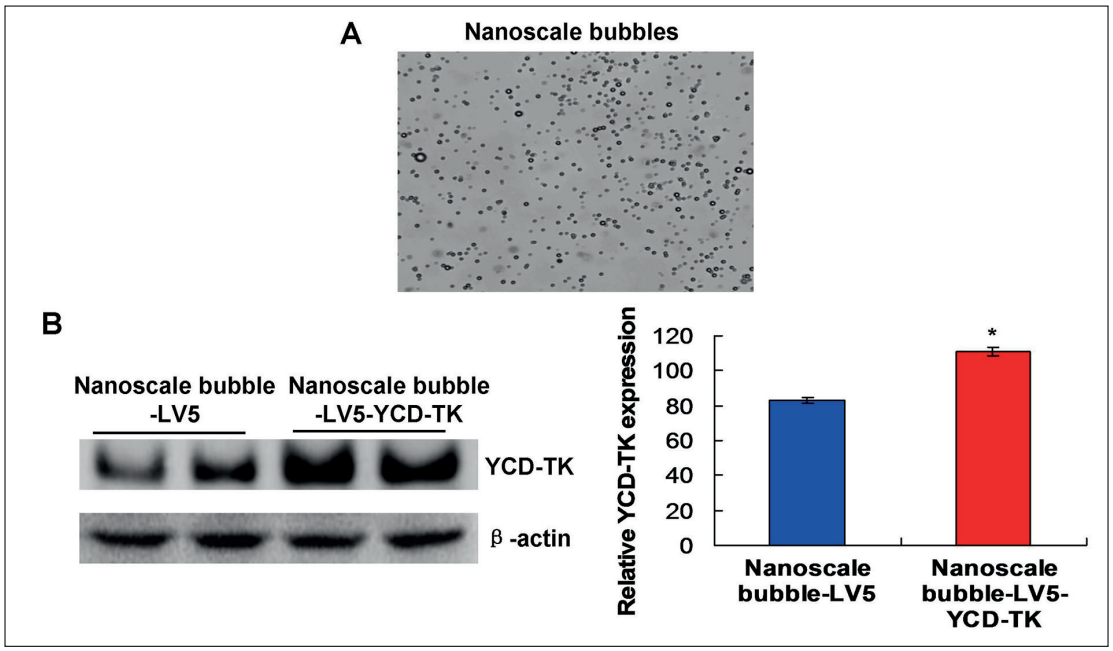

Figure 1. Nanoscale bubbles preparation and determination of YCD-TK expression. **A,** Nanoscale bubbles preparation (magnification 100 ×). **B,** Determination for YCD-TK expression using Western blot assay. **C,** Statistical analysis for YCD-TK expression. $^{*}p<0.05$ *vs.* Nanoscale bubble-LV5 group.

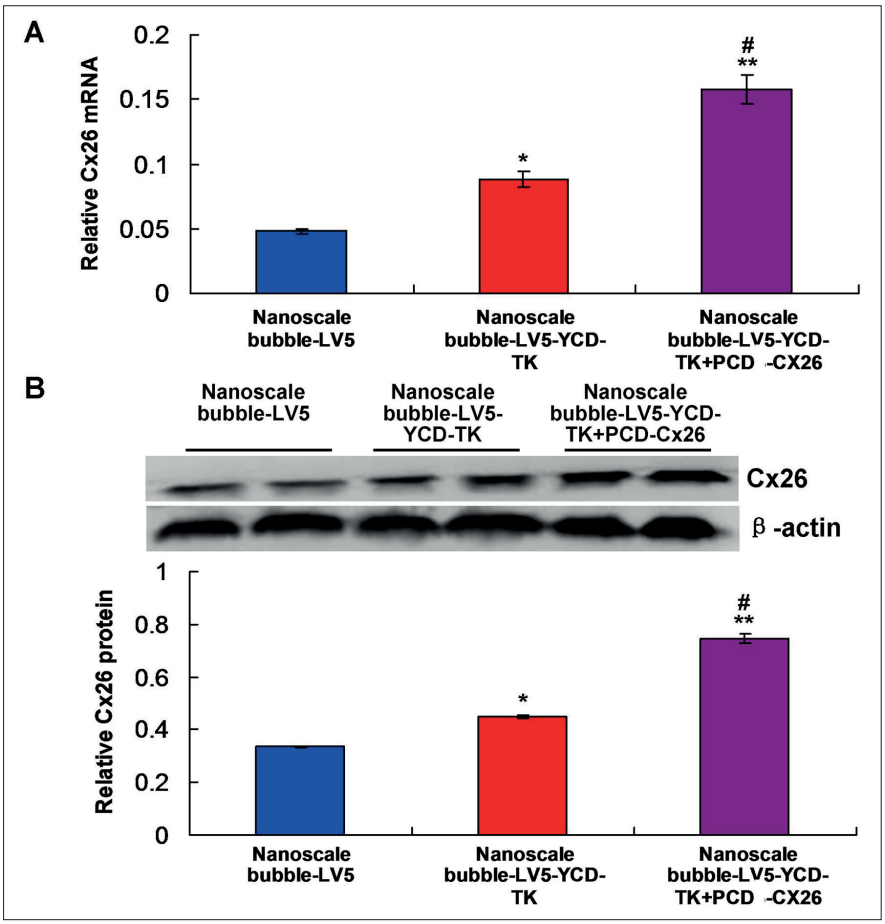

Figure 2. Determination for Cx26 mRNA and protein expression using qRT-PCR assay and Western blot assay. **A,** Cx26 mRNA expression detecting by qRT-PCR assay. **B,** Cx26 protein expression examining by Western blotting assay. **C,** Statistical analysis for the Cx26 expression. $^{*}p<0.05$, $^{**}p<0.01$ *vs.* Nanoscale bubble-LV5 group, $^{\#}p<0.05$ *vs.* Nanoscale bubble-LV5-YCD-TK group.

therefore, cell viability and apoptosis were examined using MTT analysis and flow cytometry analysis, respectively. The MTT data showed that Nanoscale bubble-LV5-YCD-TK+PCD-Cx26 demonstrated higher inhibitive rates for the cell viability compared to that of the Nanoscale bubble-LV5-YCD-TK group and Nanoscale bubble group (Figure 3A, $p<0.05$). Meanwhile, the cell viability inhibitive rates in the Nanoscale bubble-LV5-YCD-TK group were also higher compared to that in the Nanoscale bubble group (Figure 3A, $p<0.05$). Moreover, LV5-YCD-TK and PCD-Cx26 transfection (Nanoscale bubble-LV5-YCD-TK+PCD-Cx26 group) illustrated the highest levels of inhibitive rates compared to that in both the Nanoscale bubble-LV5-YCD-TK group and Nanoscale bubble group (Figure 3B, $p<0.05$). Also, Nanoscale bubble-LV5-YCD-TK treatment induced enhanced apoptosis rates compared to that in the Nanoscale bubble group (Figure 3B, $p<0.05$).

Nanoscale Bubble Delivered YCD-TK/Cx26 Expression Triggered Higher Levels of Bystander Effect

We mixed the Nanoscale bubble-mediated YCD-TK/Cx26 gene transfected BIU-87 cells and the un-transfected BIU-87 cells, to observe the YCD-TK/Cx26 triggered bystander effect. The results showed that both of YCD-TK and Cx26 gene expressions triggered the bystander effect; however, the combination of YCD-TK

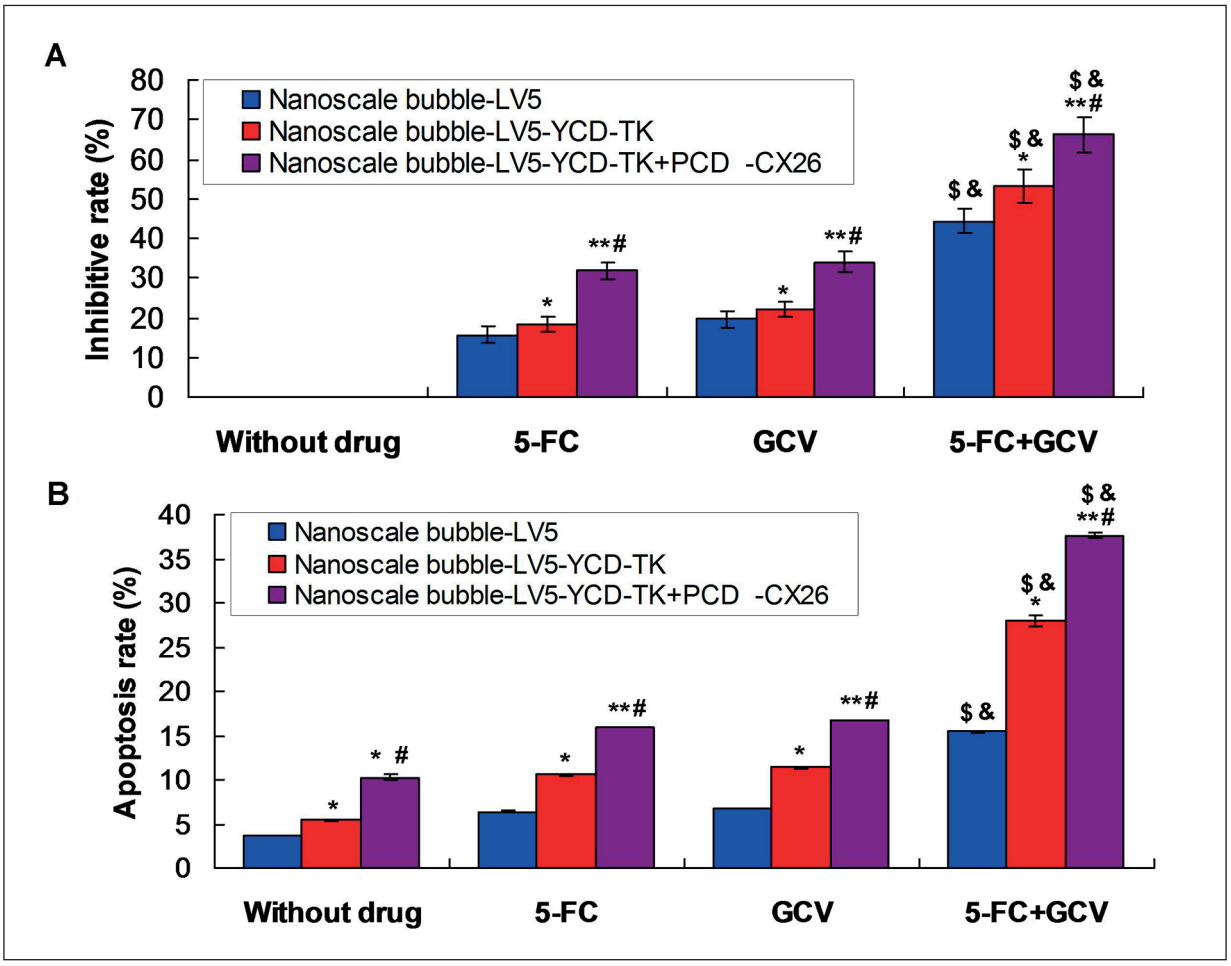

Figure 3. Evaluation for cell viability (cell inhibitive rates) and apoptosis of BIU-87 cells undergoing YCD-TK/Cx26 treatment. **A,** Analysis for the inhibitive rates according to the MTT assay recordings. **B,** Evaluation for the apoptosis of BIU-87 cells undergoing with flow cytometry assay. *$p<0.05$, **$p<0.01$ *vs.* Nanoscale bubble-LV5 group (including 5-FC, GCV, and 5-FC+GCV sub-groups). $^{\#}p<0.05$ *vs.* Nanoscale bubble-LV5+YCD-TK group (including 5-FC, GCV, and 5-FC+GCV sub-groups). $^{\$}p<0.05$ *vs.* GCV group (including Nanoscale bubble-LV5 group and Nanoscale bubble-LV5-YCD-TK group). $^{\&}p<0.05$ *vs.* 5-FC group (including Nanoscale bubble-LV5 group and Nanoscale bubble-LV5-YCD-TK group).

and Cx26 expression demonstrated the highest inhibitive rates compared to that of the single YCD-TK or Cx26 expression group (Figure 4, $p<0.05$). Furthermore, the 5-FC combining GCV treated BIU-87 cells were more sensitized to the expression of YCD-TK/Cx26 (LV5-YCD-TK+PCD-Cx26+BIU-87 group) compared to that in the LV5-YCD-TK+BIU-87 group and PCD-Cx26+BIU-87 group (Figure 4, $p<0.05$).

Nanoscale Bubble Delivered YCD-TK/Cx26 Expression Reduced Tumor Volume in Mouse Xenograft Bladder Cancer Model

After the BIU-87 cells transplantation, tumor growth in mouse Xenograft bladder cancer model was observed for 5 weeks (Figure 5A). The tumor volume in the LV5-YCD-TK+PCD-Cx26+5-FC+GCV group was significantly reduced compared to that in the LV5-YCD-TK+5-FC+GCV group, LV5-YCD-TK group, 5-FC+GCV group, and Blank group, from the 2nd week to 5th week after the transplantation (Figure 5B, $p<0.05$). Meanwhile, LV5-YCD-TK+5-FC+GCV group also illustrated a significant reduction of the tumor volume compared to that in the LV5-YCD-TK group and 5-FC+GCV group (Figure 5B, $p<0.05$). Moreover, the tumor inhibitive rate in LV5-YCD-TK+PCD-Cx26+5-FC+GCV group was significantly higher compared to that in the LV5-YCD-TK+5-FC+GCV group, LV5-YCD-TK group, 5-FC+GCV group, and Blank group (Figure 5C, $p<0.05$). These results suggest that YCD-TK combining Cx26 gene remarkably enhances the anti-tumor effects of 5-FC and GCV on the bladder cancer growth. Therefore, Nanoscale bubble delivered YCD-TK/Cx26 expression plays critical roles in inhibiting the tumor growth.

Nanoscale Bubble Delivered YCD-TK/Cx26 Expression Reduced Necrosis of Tumor Tissues in Mouse Xenograft Bladder Cancer Model

In order to clarify the reason that causes the inhibition of tumor growth, the necrosis of tumor tissues was examined using HE staining (Figure 6A). HE staining results indicated that the necrosis rate in LV5-YCD-TK+PCD-Cx26+5-FC+GCV group was significantly higher compared to that in the LV5-YCD-TK+5-FC+GCV group, LV5-YCD-TK group, 5-FC+GCV group, and Blank group (Figure 6B, $p<0.05$). Meanwhile, the LV5-YCD-TK+ 5-FC+GCV treatments also significantly enhanced the necrosis rate compared to that in the LV5-YCD-TK group and 5-FC+GCV group (Figure 6B, $p<0.05$). These results suggest that Nanoscale bubble delivered YCD-TK/Cx26 expression inhibits the tumor growth by inducing the tumor tissue necrosis.

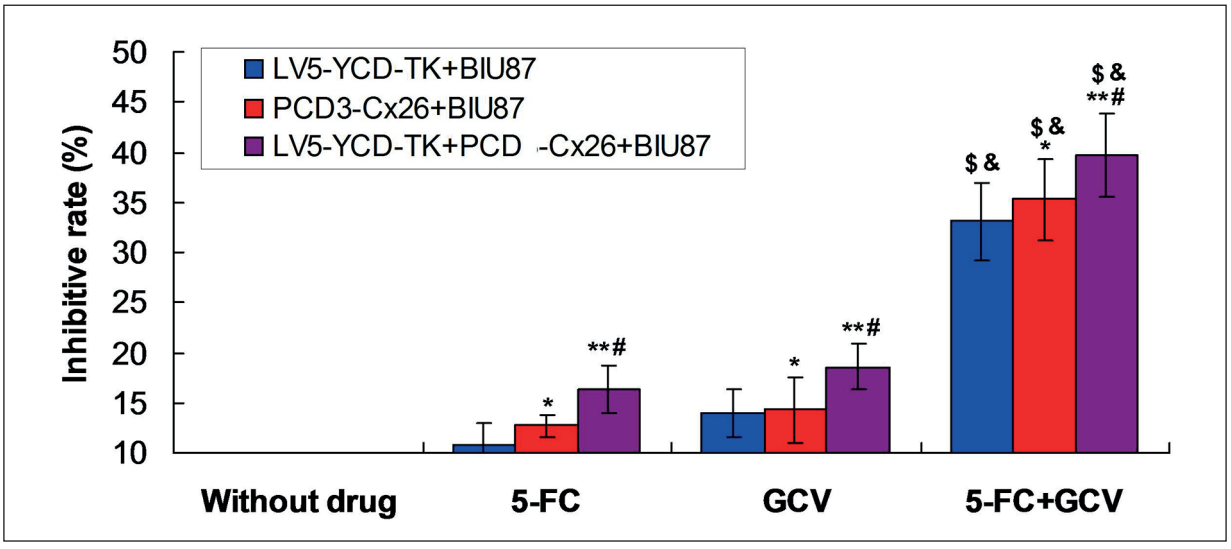

Figure 4. Identification for the YCD-TK/Cx26 transfection triggered bystander effect on the BIU-87 cells undergoing 5-FC/GCV treatment. *$p<0.05$, **$p<0.01$ *vs.* Nanoscale bubble-LV5 group (including 5-FC, GCV, and 5-FC+GCV sub-groups). #$p<0.05$ *vs.* Nanoscale bubble-LV5+YCD-TK group (including 5-FC, GCV, and 5-FC+GCV sub-groups). $$p<0.05$ *vs.* GCV group (including Nanoscale bubble-LV5 group and Nanoscale bubble-LV5-YCD-TK group). &$p<0.05$ *vs.* 5-FC group (including Nanoscale bubble-LV5 group and Nanoscale bubble-LV5-YCD-TK group).

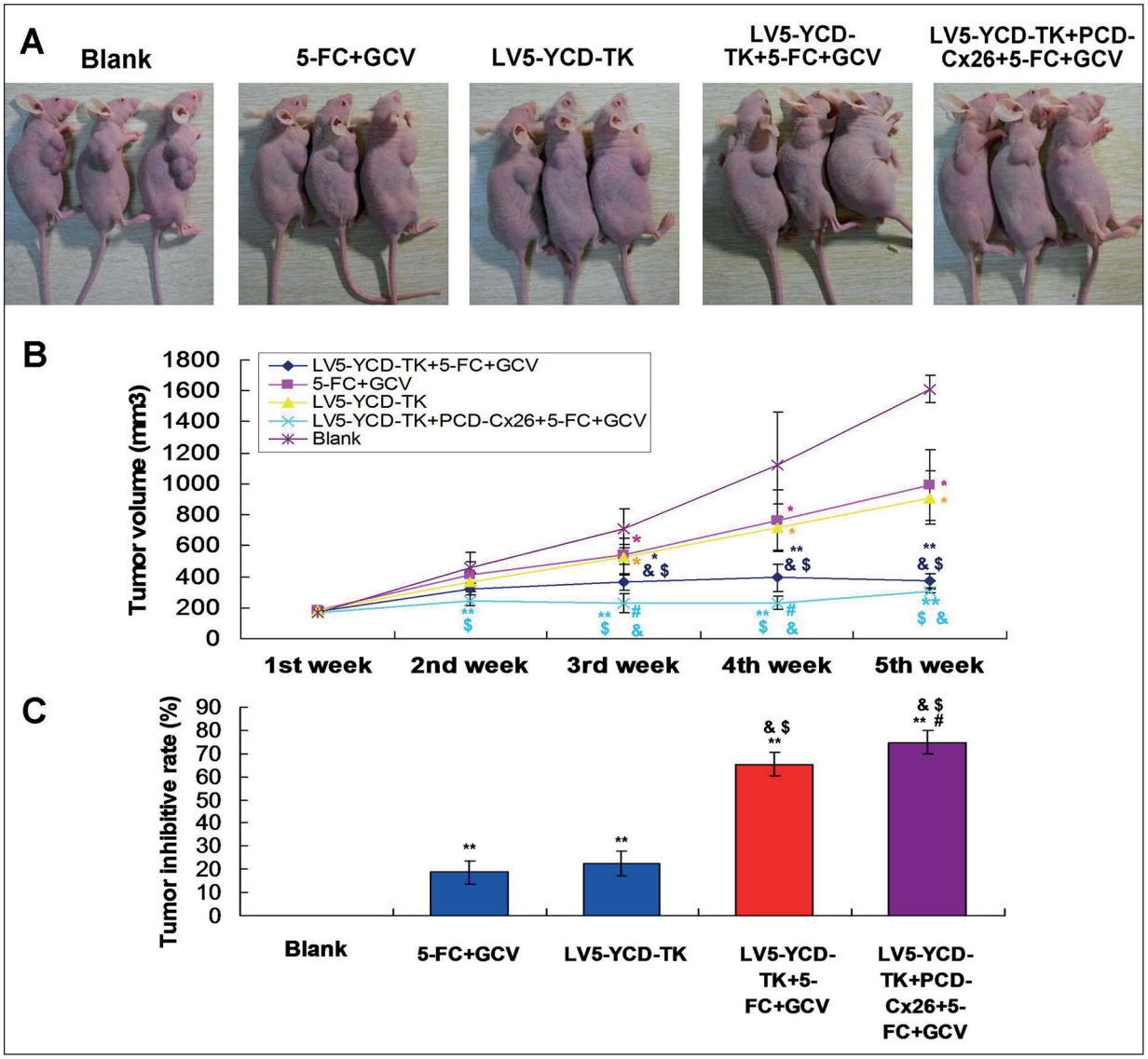

Figure 5. Tumor volume evaluation for mouse Xenograft bladder cancer model from 1st week to 5th week. **A,** Images for tumor growth in Xenograft bladder cancer mouse models. **B,** Statistical analysis for tumor volume. **C,** Statistical analysis for tumor inhibitive rates. *$p<0.05$ *vs.* LV3 group. *$p<0.05$, **$p<0.01$ *vs.* Nanoscale bubble-LV5 group (including 5-FC, GCV and 5-FC+GCV sub-groups). $^{\#}p<0.05$ *vs.* Nanoscale bubble-LV5+YCD-TK group (including 5-FC, GCV and 5-FC+GCV sub-groups). $^{\$}p<0.05$ *vs.* GCV group (including Nanoscale bubble-LV5 group and Nanoscale bubble-LV5-YCD-TK group). $^{\&}p<0.05$ *vs.* 5-FC group (including Nanoscale bubble-LV5 group and Nanoscale bubble-LV5-YCD-TK group).

Discussion

Nowadays, cancer has become the most important reason for the mortality and morbidity of patients[28]. Although a large number of cancer patients have been successfully treated using surgical resection, radio/chemotherapy, immunotherapy, the non-surgical, and non-traumatic tumor therapy technologies have been extensively explored in recent years[29,30]. Especially for gene therapy-dependent precision strategy, which has been proven to be an important approach for treating cancers[31]. Due to the limitations or associated side effects of the previous vectors, such as lower specificity and cell cytotoxicity, we employed and synthesized the Nanoscale ultrasound contrast agent, Nanoscale bubble, as the gene delivery vector[32,33].

Many studies[34,35] reported that the cytotoxic gene therapy strategy is conducted by cloning the suicide gene or the other therapeutic genes into the vectors, combining with the GCV treatment

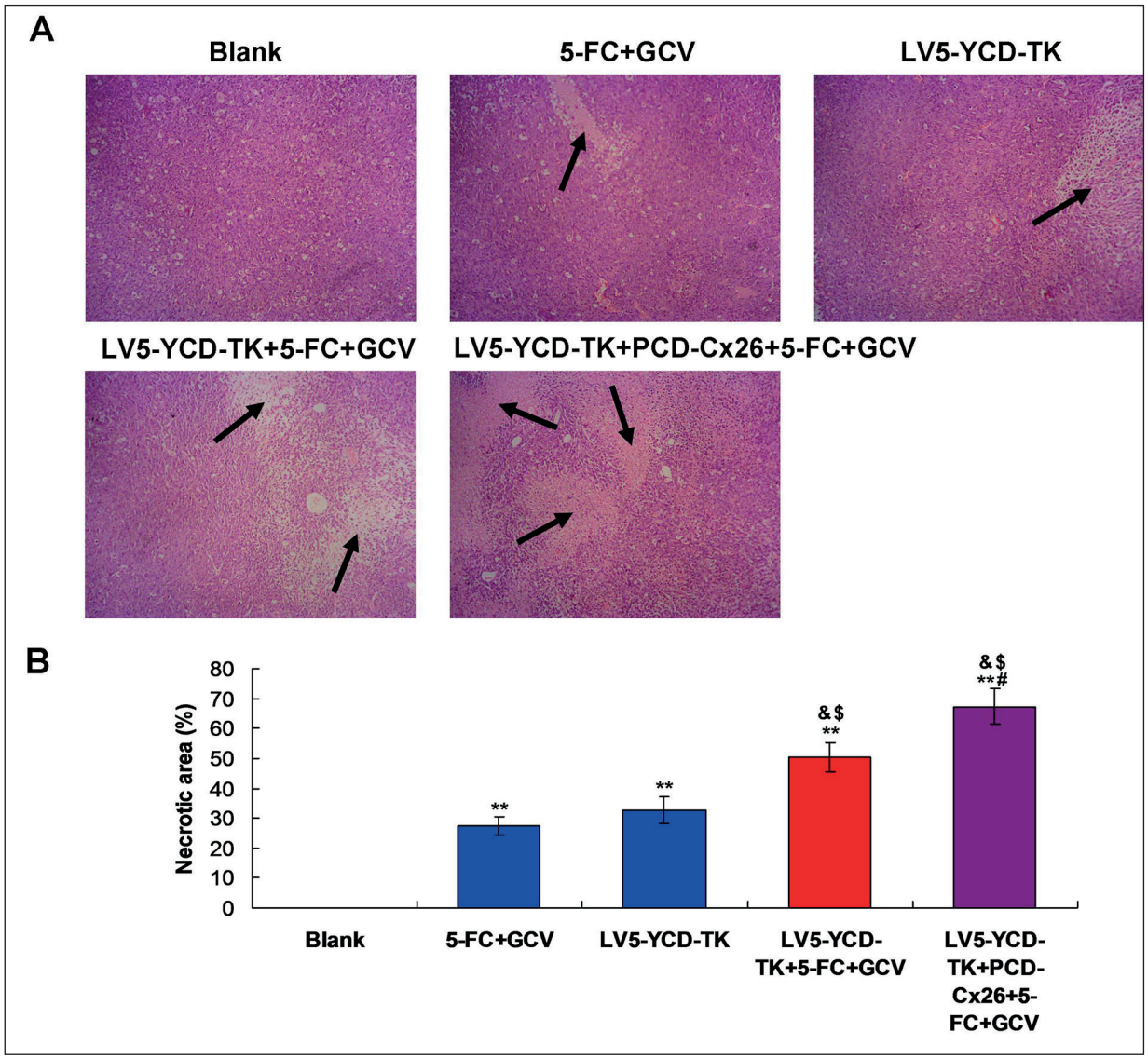

Figure 6. Examination for the necrosis of tumor tissues in the mouse Xenograft bladder cancer model using HE staining assay. **A,** HE staining images for the necrosis of tumor tissues (magnification 100 ×). **B,** Statistical analysis for the necrosis of tumor tissues. $^{**}p<0.01$ *vs.* Blank group. $^{\#}p<0.05$ *vs.* Nanoscale bubble-LV5+YCD-TK+5-FC+GCV group. $^{\$}p<0.05$ *vs.* 5-FC+GCV group. $^{\&}p<0.05$ *vs.* LV5+YCD-TK group.

together, which has been proven to be effective for suppressing the tumor cell proliferation and tumor growth. In the present study, we generated the Nanoscale babble carrying the suicide gene (YCD-TK) and tumor-suppressor gene (Cx26) and explored its effects on the tumor growth of mouse Xenograft bladder cancer model. The previous study[36] showed that the suicide gene, YCD-TK, holds the ability to convert pro-drug 5-FC to the therapeutic form as 5-fluorouracil, which could enhance the radiosensitivity of tumor cells. Therefore, LV5-YCD-TK+PCD-Cx26+5-FC+GCV therapeutic strategy was generated and applied to the mouse Xenograft bladder cancer model.

Our results indicated that both YCD-TK and Cx26 genes higher expressed in the BIU-87 cells undergoing LV5-YCD-TK+PCD-Cx26 transfection and 5-FC+GCV treatment. MTT assay results also showed that both LV5-YCD-TK+PCD-Cx26 and LV5-YCD-TK transfection significantly enhanced the inhibitive rate of BIU-87 cells undergoing 5-FC and/or GCV treatment; however, LV5-YCD-TK+PCD-Cx26 demonstrated the

most significant effects on tumor proliferation. Meanwhile, LV5-YCD-TK+PCD-Cx26 transfection, together with 5-FC combining GCV treatment, exhibited significantly higher inhibitive rates compared with that together with single 5-FC or GCV treatment. Moreover, LV5-YCD-TK+PCD-Cx26 and LV5-YCD-TK transfection into BIU-87 cells undergoing 5-FC and/or GCV treatment also induced evident apoptosis, while LV5-YCD-TK+PCD-Cx26 illustrated higher inducible effects. These findings suggest that the tumor-suppressor gene (Cx26) and suicide gene (YCD-TK) demonstrated higher anti-tumor cell proliferation effects by inducing the tumor cell apoptosis, which is consistent with the former description[37,38].

When exposing to the genotoxic administration, the tumor cells not only initiated the DNA damage response, but also released the DNA damage response-associated factors in tumor cells without expose to the genotoxic treatment; this process is named "bystander effect" for the DNA damage[39,40]. The cells released bystander factors play an important role in inhibiting the radiotherapy-correlated tumor carcinogenesis[41]; therefore, we observed the YCD-TK/Cx26 genotoxic administration induced bystander effect in the BIU-87 cells. Our results indicated that the YCD-TK/Cx26 expression induced significantly higher bystander effect in BIU-87 cells undergoing 5-FC and GCV treatment compared to that in the single YCD-TK or Cx26 expressed BIU-87 cells. This result suggests that the YCD-TK/Cx26 genotoxic administration triggers evident bystander effect, which enlarges the anti-tumor effects of the gene therapy.

The bladder cancer cell line, BIU-87 cells, transplanted mouse Xenograft model was also generated in the present study. We found that YCD-TK/Cx26 gene transfection significantly reduced tumor volume and demonstrated significantly higher tumor inhibitive rates of BIU-87 cells transplanted mouse Xenograft model compared to that in the single YCD-TK or single Cx26 gene transfection animal model. Meanwhile, compared with cells without 5-FC/GCV treatment, the YCD-TK/Cx26 gene transfection combining 5-FC/GCV treatment exhibited the highest tumor inhibitive effects on the tumor growth in the mouse Xenograft model. Therefore, we discovered the evidence that YCD-TK/Cx26 gene administration could significantly strengthen the anti-tumor effects of 5-FC/GCV in the mouse Xenograft bladder cancer model. Moreover, we also found that Nanoscale bubble delivered YCD-TK/Cx26 expression inhibits the tumor growth of animal model by inducing the tumor tissue necrosis, which is consistent with the former investigations focusing on the other cancers[42-44].

Conclusions

This study generated and identified the Nanoscale bubble delivered YCD-TK/Cx26 gene therapeutic system as a potential strategy to inhibit bladder cancer cells growth in mouse Xenograft bladder cancer model. The LV5-YCD-TK+PCD-Cx26 expression could efficiently reduce BIU-87 cell proliferation, induce apoptosis *in vitro,* and suppress the tumor growth in mouse Xenograft bladder cancer model. The anti-tumor effect on tumor growth was mediated by inducing necrosis of tumor tissues in mouse Xenograft bladder cancer model. The present data highlights the potential application of YCD-TK/Cx26 gene therapeutic system as a promising therapeutic strategy for inhibiting the bladder cancer growth.

Conflict of Interest

The Authors declare that they have no conflict of interests.

References

1) Li J, Wang AS, Wang S, Wang CY, Xue S, Guan H, Li WY, Ma TT, Shan YX. LncSNHG14 promotes the development and progression of bladder cancer by targeting miRNA-150-5p. Eur Rev Med Pharmacol Sci 2019; 23: 1022-1029.
2) Ferlay J, Soerjomataram I, Dikshit R, Eser S, Mathers C, Rebelo M, Parkin DM, Forman D, Bray F. Cancer incidence and mortality worldwide: sources, methods and major patterns in GLOBOCAN 2012. Int J Cancer 2015; 136: E359-E386.
3) Dong F, Xu T, Shen Y, Zhong S, Chen S, Ding Q, Shen Z. Dysregulation of miRNAs in bladder cancer: altered expression with aberrant biogenesis procedure. Oncotarget 2017; 8: 27547-27568.
4) Larré S, Catto JW, Cookson MS, Messing EM, Shariat SF, Soloway MS, Svatek RS, Lotan Y, Zlotta AR, Grossman HB. Screening for bladder cancer: rationale, limitations, whom to target, and perspectives. Eur Urol 2013; 63: 1049-1058.
5) Li S, Yuan S, Zhao Q, Wang B, Wang X, Li K. Quercetin enhances chemotherapeutic effect of doxorubicin against human breast cancer cells while reducing toxic side effects of it. Biomed Pharmacother 2018; 100: 441-447.

6) Sternberg CN, Bellmunt J, Sonpavde G, Siefker-Radtke AO, Stadler WM, Bajorin DF, Dreicer R, George DJ, Milowsky MI, Theodorescu D, Vaughn DJ, Galsky MD, Soloway MS, Quinn DI; International Consultation on Urologic Disease-European Association of Urology Consultation on Bladder Cancer 2012. Eur Urol 2013; 63: 58-66.

7) Schwaederle M, Zhao M, Lee JJ, Eggermont AM, Schilsky RL, Mendelsohn J, Lazar V, Kurzrock R. Impact of precision medicine in diverse cancers: a meta-analysis of phase II clinical trials. J Clin Oncol 2015; 33: 3817-3825.

8) Shen L, Liu SJ, Zhang NS, Dai GL, Zou C, Li CY, Chen XH, Ju WZ. Sensitive and selecive LC-MS/MS assay for quantitation of flutrimazole in human plasma. Eur Rev Med Pharmacol Sci 2017; 21: 2964-2969.

9) Zhang Y, Wang Z, Gemeinhart RA. Progress in microRNA delivery. J Control Release 2013; 172: 962-974.

10) Gao F, Zafar MI, Juttner S, Hocker M, Wiednmann B. Expression and molecular regulation of the Cox2 gene in gastroenteropancreatic neuroendocrine tumors and antiproliferation of nonsteroidal anti-inflammatory drugs (NSAIDs). Med Sci Monit 2018; 24: 8125-8140.

11) Giacca M, Zacchigna S. Virus-mediated gene delivery for human gene therapy. J Control Release 2012; 16: 377-388.

12) Foguer K, Braga Mde S, Peron JP, Bortoluci KR, Bellini MH. Endostatin gene therapy inhibits intratumoral macrophage M2 polarization. Biomed Pharmacother 2018; 79: 102-111.

13) Yu L, Zhang HF, Jiang DW, Zhao DY, Liu H, Shen LM. Comparison of imaging features and diagnostic values of MRI, CT and contrast-enhanced ultrasonography in the diagnosis of cervical carcinoma staging. Eur Rev Med Pharmacol Sci 2018; 22: 4784-4791.

14) Sugimoto M, Takagi T, Suzuki R, Konno N, Asama H, Watanabe K, Nakamura J, Kikuchi H, Waragai Y, Takasumi M, Sato Y, Hikichi T, Ohira H. Constrast-enhanced harmonic endoscopic ultrasonography in gallbladder cancer and pancreatic cancer. Fukushima J Med Sci 2017; 63: 39-45.

15) Yin T, Wang P, Zheng R, Zheng B, Cheng D, Zhang X, Shuai X. Nanobubbles for enhanced ultrasound imaging of tumors. Int J Nanomedicine 2012; 7: 895-904.

16) Yildirim A, Chattarai R, Blum NT, Goldscheitter GM, Goodwin AP. Stable encepsulation of air in mesoporous silica nanoparticles: fluorocarbon-free nanoscale ultrasound contrast agents. Adv Healthc Mater 2016; 5: 1290-1298.

17) Portsmouth D, Hlavaty J, Renner M. Suicide genes for cancer therapy. Mol Aspects Med 2007; 28: 4-41.

18) Tang W, He Y, Zhou S, Ma Y, Liu G. A novel Bifidobacterium infantis-mediated TK/GCV suicide gene therapy system exhibits antitumor activity in a rat model of bladder cancer. J Exp Clin Cancer Res 2009; 28: 155.

19) Graepler F, Lemken ML, Wybranietz WA, Schmidt U, Smirnow I, Gross CD, Spiegel M, Schenk A, Graf H, Lauer UA, Vonthein R, Gregor M, Armeanu S, Bitzer M, Lauer UM. Bifunctional chimeric superCD suicide gene-YCD: YUPRT fusion is highly effective in a rat hepatoma model. World J Gastroenterol 2005; 11: 6910-6919.

20) Rejiba S, Bigand C, Parmentier C, Masmoudi A, Hajri A. Oncosuppresive suidice gene virotherapy "PVH1-yCD/5-FC" for pancreatic peritoneal carcinomatosis treatment: NFkB and Akt/PI3K involvement. PLoS One 2013; 8: e70594.

21) Loncarek J, Yamasaki H, Levillain P, Milinkevitch S, Mesnil M. The expression of the tumor suppressor gene connexin 26 is not mediated by methylation in human esophageal cancer cells. Mol Carcinog 2003; 36: 74-81.

22) Suzuki R, Namai E, Oda Y, Nishiie N, Otake S, Koshima R, Hirata K, Taira Y, Utoguchi N, Nakagawa S, Maruyama K. Cancer gene therapy by IL-12 gene delivery using liposomal bubbles and tumoral ultrasound exposure. J Control Release 2010; 142: 245-250.

23) Fu YR, Chen F, Luo Y, Yi YF. Nanoscale bubble ultrasound contrast agents-mediated suicide gene therapy system, Nanoscale bubble-LV5-YCD- TK/GCV/5-FC, effectively inhibits bladder cancer cell growth. Eur Rev Med Pharmacol Sci 2019; 23: 75-86.

24) Yang H, Xiong X, Zhang L, Wu C, Liu Y. Adhesion of bio-functionalized ultrasound microbubbles to endothelial cells by targeting to vascular cell adhesion molecule-1 under shear flow. Int J Nanomedicine 2011; 6: 2043-2051.

25) Li H, Jiang X, Niu X. Long non-coding RNA reprogramming (ROR) promotes cell proliferation in colorectal cancer via affecting p53. Med Sci Monit 2017; 23: 919-928.

26) Livak KJ, Schmittgen TD. Analysis of relative gene expression data using real-time quantitative PCR and the 2(-Delta Delta C(T)) method. Methods 2001; 25: 402-408.

27) Yan P, Zhang Y, Wang C, Lv F, Song L. Interleukin-37 (IL-37) suppresses pertussis toxin-induced inflammatory myopathy in a rat model. Med Sci Monit 2018; 24: 9187-9195.

28) Bray F, Jemal A, Grey N, Ferlay J, Forman D. Global cancer transitions according to the human development index (2008-2030): a population-based study. Lancet Oncol 2012; 13: 790-801.

29) Akhtar J, Wang Z, Yu C, Zhang ZP. Effectiveness of local injection of lentivirus-delivered stathmin1 and stathmin1 shRNA in human gastric cancer xenograft mouse. J Gastroenterol Hepatol 2014; 29: 1685-1691.

30) Higashi K, Hazama S, Araki A, Yoshimura K, Lizuka N, Yoshino S, Noma T, Oka M. A novel cancer vaccine strategy with combined IL-18 and HSV-TK gene therapy driven by the hTERT promoter in a murine colorectal cancer model. Int J Oncol 2014; 45: 1412-1420.

31) Li HL, Liang S, Cui JH, Han GY. Targeting of GSK-3 beta by miR-214 to facilitate gastric cancer cell proliferation and decrease of cell apoptosis. Eur Rev Med Pharmacol Sci 2018; 22: 127-134.

32) Appaiahgari MB, Vrati S. Adenoviruses as gene/vaccine delivery vectors: promises and pitfalls. Expert Opin Biol Ther 2015; 15: 337-351.

33) Marxer EE, Brussler J, Becker A, Schummelfeder J, Schubert R, Nimsky C, Bakowsky U. Development and characterization of new nanoscaled ultrasound active lipid dispersions as contrast agents. Eur J Pharm Biopharm 2011; 77: 430-437.

34) Wang Z, Chang Z, Lu M, Shao D, Yue J, Yang D, Zheng X, Li M, He K, Zhang M, Chen L, Dong WF. Shape-controlled magnetic mesoporous silica nanoparticles for magnetically mediated suicide gene therapy of hepatocellular carcinoma. Biomaterials 2018; 154: 147-157.

35) Jiang L, Xiao X, Ren J, Tang Y, Weng H, Yang Q, Wu M, Tang W. Proteomic analysis of bladder cancer indicates Prx-I as a key molecule in BI-TK/GCV treatment system. PLoS One 2014; 9: e98764.

36) Evans DB, Pisters PW, Lee JE, Bold RJ, Charnsangavej C, Janjan NA, Wolff RA, Abbruzzese JL. Preoperative chemoradiation strategies for localized adenocarcinoma of the pancreas. J Hepatobiliary Pancreat Surg 1998; 5: 242-250.

37) Yin X, Yu B, Tang Z, He B, Ren J, Xiao X, Tang W. Bifidobacterium infantis-mediated HSV-TK/GCV suicide gene therapy induces both extrinsic and intrinsic apoptosis in a rat model of bladder cancer. Cancer Gene Ther 2013; 20: 77-81.

38) Tanaka M, Grossman HB. Connexin 26 gene therapy of human bladder cancer: induction of growth suppression, apoptosis and synergy with cisplatin. Hum Gene Ther 2001; 12: 2225-2236.

39) Martin OA, Redon CE, Nakamura AJ, Dickey JS, Georgakilas AG, Bonner WM. Systemic DNA damage related to cancer. Cancer Res 2011; 71: 3437-3441.

40) Lin X, Wei F, Major P, Al-Nedawi K, Al Saleh HA, Tang D. Microvesicles contribute to the Bystander effect of DNA damage. Int J Mol Sci 2017; 18. pii: E788.

41) Prise KM, O'Sullivan JM. Radiation-induced bystander signaling in cancer therapy. Nat Rev Cancer 2009; 9: 351-360.

42) Milosavljevic MZ, Jovanovic JP, Pejnovic NN, Mitrovic SL, Arsenijevic NN, Simovic Markovic BJ, Lukic ML. Deletion of IL-33R attenuates VEGF expression and enhances necrosis in mammary carcinoma. Oncotarget 2016; 7: 18106-18115.

43) Yin X, Zhu L, Tan W, Zhu X, Liu S, Xu W. Time intervals between prior cervical conization and posterior hysterectomy influence postoperative infection in patients with cervical intraepithelial neoplasia or cancer. Med Sci Monit 2018; 24: 9063-9072.

44) Karsch-Bluman A, Feiglin A, Arbib E, Stern T, Shoval H, Schwob O, Berger M, Benny O. Tissue necrosis and its role in cancer progression. Oncogene 2019; 38: 1920-1935.